Stimulated Raman scattering of intense laser pulses in air

J. R. Peñano, P. Sprangle, P. Serafim,* B. Hafizi,† and A. Ting
Plasma Physics Division, Naval Research Laboratory, Washington, DC 20375, USA
(Received 8 May 2003; published 24 November 2003)

Stimulated rotational Raman scattering (SRRS) is known to be one of the processes limiting the propagation of high-power laser beams in the atmosphere. In this paper, SRRS, Kerr nonlinearity effects, and group velocity dispersion of short laser pulses and pulse trains are analyzed and simulated. Fully time-dependent, three-dimensional, nonlinear propagation equations describing the Raman interaction, optical Kerr nonlinearity due to bound electrons, and group velocity dispersion are presented and discussed. The effective time-dependent nonlinear refractive index containing both Kerr and Raman processes is derived. Linear stability analysis is used to obtain growth rates and phase matching conditions for the SRRS, modulational, and filamentation instabilities. Numerical solutions of the propagation equations in three dimensions show the detailed evolution of the Raman scattering instability for various pulse formats. The dependence of the growth rate of SRRS on pulse duration is examined and under certain conditions it is shown that short ($\sim$psec) laser pulses are stable to the SRRS instability. The interaction of pulses in a train through the Raman polarization field is also illustrated.

DOI: 10.1103/PhysRevE.68.056502 PACS number(s): 41.60.Cr, 42.65.Dr, 42.68.Mj, 42.65.Re

I. INTRODUCTION

Recent advances in laser technology have generated tremendous opportunities for applications which require the propagation of high-intensity, short laser pulses through the atmosphere. For example, free electron lasers (FELs) have the potential for both high peak power and higher average power than existing systems, along with a flexible pulse format [1]. FELs capable of delivering megawatts of average power are in the foreseeable future. The pulse train of a MW-class FEL driven by a radio frequency (RF) linac will likely be characterized by individual pulses with durations of ~ 1 psec, peak powers in the GW range, separated by ~ 1 nsec. These short, high intensity laser pulses can undergo unique interactions with the atmosphere in which both linear and nonlinear processes play a central role [2]. As a result of the high intensities, bound electron anharmonicity (optical Kerr effect) and stimulated rotational Raman scattering (SRRS) can affect laser beam propagation. Because of the short duration of these pulses, group velocity dispersion (GVD) can also significantly affect propagation.

SRRS of a laser pulse in air is a quantum mechanical process involving the excitation of the rotational states of the molecular constituents of air by the laser pulse. It can be characterized as an instability that scatters laser energy into multiple Stokes and anti-Stokes frequency bands [3] which, because of the dispersive properties of air, can propagate at different velocities and at large angles with respect to the initial laser pulse, causing a severe distortion of the laser envelope [4]. Theoretically, SRRS can be understood as a three-level interaction [3,5] through the energy level diagrams shown in Fig. 1. The molecular scatterer is assumed to have two rotational eigenstates, 1 (the ground state) and 2, with corresponding energies W_1 and W_2, and an excited state, e.g., an electronic or translational state, with energy $W_3 \gg W_2 - W_1$. In this paper we consider the nonresonant scattering process in which the central laser frequency $\omega_0 \neq \Omega_{31}$, Ω_{32}, where $\Omega_{nm} = \Omega_n - \Omega_m$, and Ω_n is the frequency associated with state n. It is also assumed that Ω_{31}, $\Omega_{32} \gg \omega_0 \gg \omega_R$, where $\omega_R \equiv \Omega_{21}$ is defined as the rotational frequency. In this situation, state 3 is not populated and the laser excites a virtual state which can decay to produce the Stokes and anti-Stokes radiation. The generation of Stokes radiation consists of a transition from state (1) to a virtual state followed by a transition from the virtual state to state (2). In the process, a photon with frequency $\omega_- = \omega_0 - \omega_R$ is emitted. The generation of anti-Stokes radiation consists of a transition from state (2) to a virtual state followed by a transition from the virtual state to state (1), thereby emitting a photon at frequency $\omega_+ = \omega_0 + \omega_R$. Since the population of state (2) is much smaller than that of state (1) in thermal equilibrium, the anti-Stokes lines are generally much weaker than the Stokes lines [3].

Stimulated Raman scattering of laser pulses propagating through air had been studied extensively in the 1980s for longer ($\sim$nsec) laser pulses [6–10]. For altitudes below 100

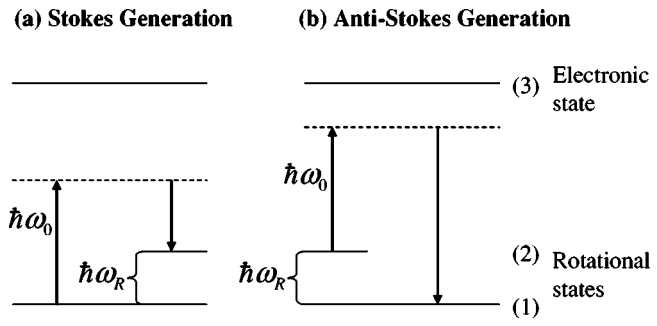

FIG. 1. Energy level diagram of Stokes and anti-Stokes line generation from a three-level model of stimulated rotational Raman scattering (SRRS).

*Present address: Northeastern University, Department of Electrical Engineering, Boston, MA 02115.

†Present address: Icarus Research, Bethesda, MD.

km, the dominant Raman process for nsec pulses is due to scattering from N_2 molecules involving the S(8) rotational transition from the $J=8$ to $J=6$ rotational states, while the molecule remains in the vibrational ground state [11]. For a linearly polarized laser with wavelength 1 μm, experiments using nsec pulses indicate that the Raman gain coefficient is ~ 2.5 cm/TW [7]. The observed Raman shift for the S(8) rotational transition is $75\,\mathrm{cm}^{-1}$ ($\omega_R \sim 1.4\times 10^{13}\ \mathrm{sec}^{-1}$) while the characteristic relaxation time for excited states is typically 0.1 nsec at sea level [9]. A number of more recent experimental studies have employed ultrashort ($\sim$100 fsec) laser pulses to investigate Raman scattering in air and various gasses [12]. In particular, the gain coefficient and damping rate have been measured and found to be different from those appropriate for longer pulses. The Raman scattering process for short pulses in air is expected to be markedly different from long pulse scattering [13,14]. For example, the spectral width of a picosecond FEL pulse is comparable with the typical rotational frequency. Hence there is an appreciable signal at the Stokes frequency from the onset. Hence, the number of e-foldings that the Stokes wave must undergo before it becomes comparable with the carrier signal amplitude is reduced relative to the number of e-foldings required for a longer nanosecond pulse. Group velocity dispersion is also important for picosecond pulses propagating kilometer distances in air. The longitudinal spreading and frequency redistribution associated with group velocity dispersion can affect the Raman process.

In a pulse train, intrapulse interactions may also modify the Raman process. The leading pulses can excite molecular rotations which have a finite relaxation time. If the pulse separation in time is not large compared with the relaxation time, subsequent pulses will encounter a perturbed medium, which could either enhance or suppress the Raman interaction of the trailing pulse.

One purpose of this paper is to present and discuss a theoretical model that takes into account these and other processes that govern the propagation of intense, short laser pulses in air. A closed system of equations is derived that describes the three-dimensional, fully time-dependent propagation of a laser pulse along with the self-consistent evolution of the rotational Raman polarization field. The propagation equation also includes the effects of group velocity dispersion, bound electron anharmonicity (optical Kerr effect), and nonparaxial propagation. In some limits an analytical form for the effective nonlinear refractive index can be derived. For laser pulses that are short compared with the rotational period, this index is simply due to bound electron anharmonicity since the rotational levels cannot be excited. For longer laser pulses, the Kerr and Raman effects both contribute to the nonlinear index and are of the same order [15].

Turbulence and ionization, which can also be important effects in the propagation of short, high-intensity pulses, has been discussed in other related articles [2,15]. For the purpose of this study, however, these other effects are neglected in order to isolate the Raman process.

A full-scale, three-dimensional (3D) numerical simulation which solves the propagation equations presented in this paper has been developed at NRL. Because the simulation is fully time dependent and self-consistent, it is capable of modeling the transient short-pulse Raman interaction and the consequent generation of broad multiwave spectra, as well as the more standard, long pulse interaction. Simulations are used to model in detail the propagation of laser pulses of various formats undergoing SRRS and the dependence of the Raman instability growth rate on laser pulse length is investigated. The atmospheric propagation of a pulse train is also considered. In one example, a pulse train characteristic of a MW-class FEL is modeled. Numerical results illustrate the interaction of pulses through the Raman polarization field.

This paper is organized as follows. In Sec. II the nonlinear atmospheric propagation equations are derived. The effective nonlinear index due to the Raman process is derived in Sec. III. Section IV analyzes the various small signal gain mechanisms included in the theoretical model, i.e., stimulated Raman, modulational, and filamentation instabilities. Section V presents the results of the numerical simulations. Conclusions are presented in Sec. VI.

II. NONLINEAR PROPAGATION EQUATIONS

An intense laser pulse propagating through the atmosphere is subject to a number of linear and nonlinear processes which include diffraction, group velocity dispersion (GVD), and nonlinearities due to the polarization field associated with bound electrons and stimulated molecular Raman scattering. A general equation describing the atmospheric propagation of a laser pulse subject to these effects is outlined in this section. The details of the derivation will be published elsewhere. The starting point is the wave equation for the laser electric field $\mathbf{E}(\mathbf{r},t)$, given by

$$\left(\nabla_\perp^2 + \frac{\partial^2}{\partial z^2} - \frac{1}{c^2}\frac{\partial^2}{\partial t^2}\right)\mathbf{E} = \frac{4\pi}{c^2}\frac{\partial^2 \mathbf{P}}{\partial t^2}, \tag{1}$$

where $\nabla_\perp^2$ is the transverse Laplacian operator and z is the coordinate in the direction of propagation.

The polarization field is written as the sum of a linear and nonlinear contribution, $\mathbf{P}=\mathbf{P}_L+\mathbf{P}_{NL}$. The laser electric field, $\mathbf{E}(\mathbf{r},t)$ is written in terms of a complex amplitude and a rapidly varying phase, i.e.,

$$\mathbf{E}(\mathbf{r},t) = A(\mathbf{r},t)\exp[i\psi(z,t)]\hat{\mathbf{e}}_x/2 + \text{c.c.}, \tag{2}$$

where $A(\mathbf{r},t)$ is the complex amplitude, $\psi(z,t)=k_0 z-\omega_0 t$ is the phase, k_0 is the carrier wave number, ω_0 is the carrier frequency, $\hat{\mathbf{e}}_x$ is a transverse unit vector in the direction of polarization, and c.c. denotes the complex conjugate.

A closed system of equations is obtained by expressing the polarization field in terms of the laser electric field amplitude A. The linear polarization field modifies the refractive index while its derivatives with respect to frequency lead to temporal dispersion. The nonlinear polarization field is a consequence of bound electron anharmonicity (Kerr effect) and molecular rotation (stimulated Raman scattering effect). In terms of the linear susceptibility $\hat{\chi}_L(\omega)$, the linear polarization field is $\hat{P}_L(\omega)=\hat{\chi}_L(\omega)\hat{E}(\omega)$, where the overhat de-

notes the temporal Fourier transform. The amplitude of the nonlinear polarization field can be written as a sum of P_K due to the optical Kerr effect of bound electrons and P_R due to stimulated Raman scattering from N_2 molecules. The nonlinear Kerr and Raman polarization fields are, respectively,

$$P_K(\mathbf{r},t)=\frac{cn_0^2n_K}{16\pi^2}|A(\mathbf{r},t)|^2A(\mathbf{r},t), \tag{3a}$$

$$P_R(\mathbf{r},t)=\chi_L Q(\mathbf{r},t)A(\mathbf{r},t), \tag{3b}$$

where n_K is the nonlinear index coefficient due to the Kerr effect, $\chi_L \equiv \hat{\chi}_L(\omega_0)$ is the linear susceptibility evaluated at ω_0, and $Q(\mathbf{r},t)$ is the unitless Raman polarization function which satisfies Eqs. (5) given below. Using Eqs. (1)–(3), the following propagation equation can be derived (see Appendix A):

$$\left(\nabla_\perp^2+2ik_0\frac{\partial}{\partial z}-\frac{2}{v_g}\frac{\partial^2}{\partial z\partial\tau}-k_0\beta_2\frac{\partial^2}{\partial\tau^2}\right)A(\mathbf{r},\tau)$$
$$=-2\frac{\omega_0^2}{c^2}\left(\frac{cn_0^2n_K}{8\pi}|A|^2+2\pi\chi_L Q(\mathbf{r},\tau)\right)A(\mathbf{r},\tau). \tag{4}$$

In Eq. (4), $k_0=n_0(\omega_0)\omega_0/c$, $n_0(\omega_0)=(1+4\pi\chi_L)^{1/2}$ is the linear refractive index, and β_2 is the group velocity dispersion (GVD) parameter. In writing Eq. (4) the independent variables $(z,\ t)$ have been changed to the pulse frame variables (z,τ) where $\tau=t-z/v_g$, v_g is the linear group velocity of the laser pulse, and $\beta_g=v_g/c$. For air at one atmosphere and laser wavelengths of $\lambda\sim1\ \mu$m, we note that $\chi_L\sim5\times10^{-5}$ and $\beta_2\sim1.6\times10^{-31}$ sec^2/cm. Equation (4) describes the 3D propagation of a laser pulse in a dispersive nonlinear medium, characterized by the GVD parameter β_2, nonlinear refractive index n_K (Kerr effect), and stimulated Raman response function $Q(\mathbf{r},\tau)$.

Stimulated Raman scattering can arise through the interaction of the laser with the dipole moments of the molecular constituents of air (principally N_2 and O_2). The interaction may be analyzed quantum mechanically using a three-level model [3,5,15]. The result of this analysis (see Appendix B) is a pair of equations for the Raman response function $Q(\mathbf{r},\tau)$ and the population inversion function $W(\tau)$ given by

$$\frac{\partial^2Q}{\partial\tau^2}+\Omega_0^2Q+2\Gamma_2\frac{\partial Q}{\partial\tau}=-\frac{\mu^2}{\hbar^2}\frac{\omega_R}{\Omega}W|A|^2, \tag{5a}$$

$$\frac{\partial W}{\partial\tau}=\frac{\mu^2/\hbar^2}{\omega_R\Omega}\left(\frac{\partial Q}{\partial\tau}+\Gamma_2Q\right)|A|^2-\Gamma_1(1+W), \tag{5b}$$

where $\Omega_0^2=\omega_R^2+\Gamma_2^2$, ω_R is the fundamental rotational frequency, μ is the effective dipole moment, Γ_1 and Γ_2 are phenomenological damping rates (Γ_1 is the population relaxation rate and Γ_2 is the dipole dephasing rate) and $\Omega\equiv\Omega_{32}\approx\Omega_{31}$ is the frequency associated with transition from a higher energy virtual state (state 3) to one of two lower energy rotational states (states 1 and 2).

III. NONLINEAR INDEX DUE TO RAMAN AND KERR EFFECTS

The Kerr and Raman nonlinearities contribute to the refractive index and can thus affect the propagation of the laser pulse. The Kerr nonlinearity is associated with self-phase modulation and nonlinear self-focusing, while the stimulated Raman process can lead to the generation of multiple Stokes and anti-Stokes waves which can propagate at large angles with respect to the propagation axis, thus scattering the laser energy [4]. In this section the total nonlinear refractive index with both Kerr and Raman contributions is derived.

Retaining only the nonlinear propagation terms, and taking the one-dimensional (1D) limit ($\nabla_\perp=0$) Eq. (4) can be written as

$$2ik_0\frac{\partial A(z,\tau)}{\partial z}=-[n^2(z,\tau)-n_0^2]\frac{\omega_0^2}{c^2}A(z,\tau), \tag{6}$$

where n is the total refractive index in configuration space and n_0 is the linear index. The total time-dependent nonlinear index is identified as

$$\delta n(z,\tau)=n(z,\tau)-n_0\approx n_KI(z,\tau)+\frac{2\pi\chi_L}{n_0}Q(z,\tau) \tag{7}$$

which contains contributions from both the Kerr and Raman effects. In Eq. (7), $I(z,\tau)=cn_0|A(z,\tau)|^2/8\pi$ is the laser intensity. In the limit $\Omega_R^2\ll\Omega\Omega_0$, where $\Omega_R=\mu A_0/\hbar$ is the Rabi frequency associated with the peak electric field amplitude, A_0, the population inversion associated with stimulated Raman scattering can be neglected, i.e., $W\approx-1$, and the Raman response function, from solving Eq. (5a), is given by [16]

$$Q(z,\tau)=\frac{\mu^2}{\hbar^2}\frac{1}{\Omega}\int_0^\tau d\tau'\exp[-\Gamma_2(\tau-\tau')]$$
$$\times\sin[\omega_R(\tau-\tau')]|A(z,\tau')|^2. \tag{8}$$

The contribution of the Kerr effect to the polarization field is third order in the field amplitude. However, as seen from Eqs. (5)–(7), the Raman polarization field also has a contribution which is third order in the field amplitude and thus can contribute to the nonlinear refractive index at the same order as the Kerr effect. In the absence of Raman effects, the Kerr nonlinearity by itself can produce a modulational instability when the GVD parameter $\beta_2<0$ [17].

As an example, consider a constant amplitude laser pulse with duration τ_L. The field amplitude can be written as $A=A_0[\Theta(\tau)-\Theta(\tau-\tau_L)]$, where $\tau=t-z/c$. From Eqs. (7) and (8), the nonlinear index within the pulse, i.e., $0<\tau<\tau_L$, is $\delta n=n_{NL}I$, where the effective coefficient of nonlinearity is given by

$$n_{NL}=n_K+n_R\{1-e^{-\Gamma_2\tau}[\cos(\omega_R\tau)+(\Gamma_2/\omega_R)\sin(\omega_R\tau)]\}, \tag{9}$$

with

$$n_R=(4\pi/n_0)^2\chi_L\frac{\omega_R}{\Omega}\frac{\mu^2}{\hbar^2\Omega_0^2 c}. \tag{10}$$

In the long pulse limit ($\tau\gg 1/\Gamma_2$), the total nonlinear coefficient is given by $n_{NL}=n_K+n_R$, i.e., n_R represents the effective coefficient of nonlinearity due to Raman effects. For pulses short compared with the characteristic Raman times ($\tau\ll 1/\omega_R$, $\tau\ll 1/\Gamma_2$), the nonlinear refractive index is due to purely the bound electron response, i.e., $n_{NL}=n_K$.

IV. GAIN MECHANISMS

Equations (4) and (5) can describe several physical mechanisms by which small amplitude perturbations on a laser beam can be amplified. In this section, a linear stability analysis is used to derive the growth rates for the stimulated Raman instability, modulational instability (MI), and filamentation instability (FI). To proceed with the analysis, the laser electric field amplitude and the Raman oscillator function are perturbed about a uniform (CW) equilibrium, i.e., $A=A_0+\delta A$ and $Q=Q_0+\delta Q$ where the equilibrium quantities are given by

$$A_0(z)=|A_0|\exp\left[\frac{i\omega_0^2 n_0}{k_0 c^2}(n_K+n_R)I_0 z\right], \tag{11}$$

$$Q_0=n_0 n_R I_0/(2\pi\chi_L), \tag{12}$$

where $I_0=cn_0|A_0|^2/8\pi$ denotes the pump intensity. By equilibrium, it is meant that $\partial|A_0|^2/\partial z=0$ so that the pump intensity remains constant. The perturbed quantities are written in the form

$$\delta A(z,\tau)=A_-(z)\exp[-i(k_\perp x+k_- z-\omega\tau)] + A_+(z)\exp[i(k_\perp x+k_+ z-\omega\tau)] \tag{13a}$$

and

$$\delta Q(\tau)=\tfrac{1}{2}\{\hat{Q}(z)\exp[-i(k_\perp x-\omega\tau)]+\hat{Q}^*(z) \times\exp[i(k_\perp x-\omega\tau)]\}, \tag{13b}$$

where A_- denotes the Stokes wave amplitude, A_+ denotes the anti-Stokes wave amplitude, and ω, $k_\perp$, and $k_\pm$ are real.

In the analysis that follows, it is assumed that $|\delta A|\ll|A_0|$, and that there is negligible population inversion, i.e., $W=-1$. Linearizing Eqs. (4) and (5) with respect to the perturbed quantities, the Stokes and anti-Stokes fields are found to satisfy the coupled equations (see Appendix C)

$$\frac{\partial A_+(z)}{\partial z}=G_+[A_+(z)+A_-^*(z)\exp(i\Delta kz)], \tag{14a}$$

$$\frac{\partial A_-(z)}{\partial z}=G_-[A_-(z)+A_+^*(z)\exp(i\Delta kz)], \tag{14b}$$

where

$$G_\pm\equiv i\frac{\omega_0}{c}\left(1\pm\frac{\omega}{k_0 v_g}\right)^{-1}\left(n_K+n_R\frac{\Omega_0^2}{\Omega_0^2-\omega^2\mp 2i\Gamma_2\omega}\right)I_0, \tag{15}$$

$$\Delta k=2\kappa_0-\frac{(k_0\beta_2\omega^2-k_\perp^2+2k_0\kappa_0)}{k_0(1-\omega^2/k_0^2 v_g^2)}, \tag{16}$$

and $\kappa_0=\omega_0(n_K+n_R)I_0/c$. In deriving Eqs. (14), the dispersion relations $k_0=n_0\omega_0/c$ and

$$k_\pm=\pm\frac{k_0\beta_2\omega^2-k_\perp^2+2k_0\kappa_0}{2k_0(1\pm\omega/k_0 v_g)} \tag{17}$$

are invoked. The general solution of Eqs. (14) is (see Ref. [3] and Appendix C)

$$A_-(z)=[a_+\exp(g_+ z)+a_-\exp(g_- z)]\exp(i\Delta kz/2), \tag{18}$$

$$A_+^*(z)=[b_+\exp(g_+ z)+b_-\exp(g_- z)]\exp(-i\Delta kz/2), \tag{19}$$

where the constants $a_\pm$ and $b_\pm$ denote the complex amplitudes of the eigenmodes whose growth rates are given by

$$g_\pm=\frac{1}{2}\left\{G_-+G_+^*\pm\left[(G_-+G_+^*)^2 -2i\Delta k\left(G_--G_+^*-i\frac{\Delta k}{2}\right)\right]^{1/2}\right\}. \tag{20}$$

The constants $a_\pm$ and $b_\pm$ are related by

$$b_\pm=\left(\frac{g_\pm+i(\Delta k/2)-G_-}{G_-}\right)a_\pm, \tag{21}$$

and can be written in terms of the initial ($z=0$) amplitudes $A_-(0)$ and $A_+(0)$ as

$$a_\pm=\mp\frac{1}{g_+-g_-}\{[g_\mp+i(\Delta k/2)-G_-]A_-(0)-G_-A_+^*(0)\}, \tag{22}$$

$$b_\pm=\pm\frac{1}{g_+-g_-}\{[g_\pm+i(\Delta k/2)-G_-]A_+^*(0)+G_+^*A_-(0)\}. \tag{23}$$

We now consider several limiting cases of Eqs. (18)–(23).

A. Stimulated rotational raman scattering (SRRS)

Stimulated Raman scattering, in general, is associated with the generation of both Stokes (frequency down-shifted) and anti-Stokes (frequency up-shifted) radiation. For laser pulses with durations much longer than the rotational period, the conversion of energy from the carrier field (pump) to the Stokes and anti-Stokes sidebands proceeds as a parametric instability in which the Stokes and anti-Stokes waves can be strongly or weakly coupled. For a CW pump, Eqs. (20) and

(21) can be used to obtain simple expressions for the Raman growth rates in the strongly coupled and weakly coupled regimes.

For rotational Raman scattering in air of lasers with wavelength $\sim 1\ \mu$m, it is a good approximation to take $v_g \approx c$ and $\Omega_0 \ll \omega_0$. It is also a good approximation to set $\omega \approx \Omega_0$ to obtain the peak growth rate. With these approximations, the coefficients $G_\pm$ reduce to

$$G_\pm \approx \mp G_0 (1 \mp i\delta)(1 \pm \Omega_0/\omega_0)^{-1}, \tag{24}$$

where $G_0 \equiv n_R I_0 (\Omega_0/2\Gamma_2)(\omega_0/c)$, and $\delta \equiv (n_K/n_R)(2\Gamma_2/\Omega_0)$. For rotational Raman scattering in air, $\delta \ll 1$. Using Eq. (24), the growth rates reduce to

$$g_\pm \approx -G_0 \frac{\Omega_0}{\omega_0}(1+i\delta) \pm \left\{ \left[G_0 \frac{\Omega_0}{\omega_0}(1+i\delta) \right]^2 - \frac{i\Delta k}{2}\left[2G_0(1+i\delta) - \frac{i\Delta k}{2} \right] \right\}^{1/2}, \tag{25}$$

where the phase mismatch parameter from Eq. (16) is

$$\Delta k \approx (k_\perp^2/k_0) - \beta_2 \Omega_0^2 - 2\kappa_0 (\Omega_0/\omega_0)^2. \tag{26}$$

In the limit of large phase mismatch ($\Delta k \gg G_0$) the Stokes and anti-Stokes waves are weakly coupled and the growth rates for the various eigenmodes are given by

$$g_\pm \approx \mp \mathrm{sgn}(\Delta k) G_0 \pm i(|\Delta k|/2). \tag{27}$$

Hence, the quantity $G_0 \equiv n_R I_0 (\Omega_0/2\Gamma_2)(\omega_0/c)$ is the spatial growth rate for the Raman instability in the weakly coupled regime. For a CW pump laser, the Raman gain coefficient, defined as $g_0 \equiv G_0/I_0$, can now be expressed in terms of the Raman index, i.e., $g_0 = n_R(\Omega_0/2\Gamma_2)(\omega_0/c)$. For a long ($\sim$nsec) laser pulse with $\sim 1\ \mu$m wavelength, the experimentally determined value for the gain is $g_0 = 2.5$ cm/TW [7]. For $\omega_R \sim 1.4\times 10^{13}$ sec^{-1} and $\Gamma_2 \sim 10^{10}$ sec^{-1} [9], the nonlinear index for the rotational Raman processes is $n_R = 5.6\times 10^{-20}$ cm^2/W [15].

For $\Delta k > 0$ in the weakly coupled regime, the Stokes and anti-Stokes amplitudes, from Eq. (21), are related by $(b_+/a_+) \approx i(\Delta k/G_0) \gg 1$ and $b_-/a_- \approx -i\delta \to 0$, indicating that the exponentially growing mode [$\exp \sim (g_- z)$] is primarily composed of the Stokes wave, i.e., for $G_0 z > 1$, the Stokes and anti-Stokes waves are given by $A_-(z) \approx a_- \exp(G_0 z)$ and $A_+^*(z) \approx b_- \exp(G_0 z)\exp(-2i\Delta k z)$, with $|A_-|/|A_+| \gg 1$. Similarly for $\Delta k < 0$, we find $(b_+/a_+) \approx -i\delta \to 0$, and $(b_-/a_-) \approx i(\Delta k/G_0) \gg 1$, indicating that the exponentially growing mode ($\sim e^{g_+ z}$) is again dominated by the Stokes wave.

In the limit of small phase mismatch, i.e., $G_0(\Omega_0/\omega_0) \ll \Delta k \ll G_0$, the Stokes and anti-Stokes waves are strongly coupled and the growth rate is reduced relative to the uncoupled regime. The growth rates are given by

$$g_\pm \approx \mp [1 - i\,\mathrm{sgn}(\Delta k)](2|\Delta k| G_0)^{1/2}, \tag{28}$$

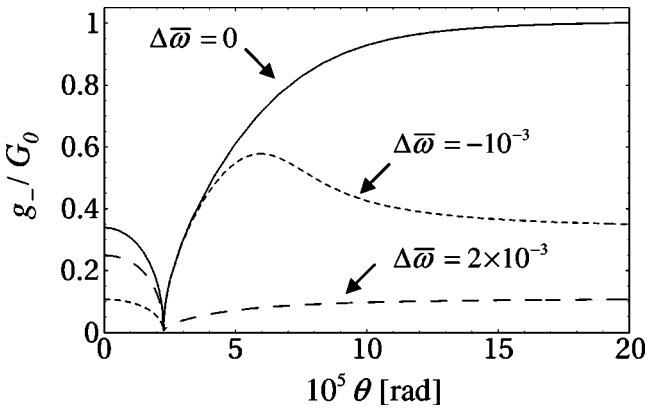

FIG. 2. Growth rate vs propagation angle for $\Delta\bar{\omega} = -10^{-3}$, 0, 2×10^{-3} where the frequency mismatch is defined as $\Delta\bar{\omega} \equiv (\omega - \Omega_0)/\Omega_0$ and the angle θ is measured with respect to the z axis. The growth rate is calculated using Eq. (20) with $n_R = n_K = 3\times 10^{-19}$ cm^2/W, $\Omega_0 = 1.4\times 10^{13}$ sec^{-1}, $\Gamma_2 = 10^{10}$ sec^{-1}, $\beta_2 = 1.6\times 10^{-31}$ s^2/cm, $I_0 = 10^7$ W/cm^2, $\lambda = 1\ \mu$m.

with the eigenmode amplitudes given by $b_\pm/a_\pm \approx -1 \mp [1 - i\,\mathrm{sgn}(\Delta k)](2|\Delta k|/G_0)$. Hence, the strongly coupled regime is characterized by reduced growth with the Stokes and anti-Stokes waves having roughly equal amplitudes.

In the limit of perfect phase matching ($\Delta k = 0$) there is no exponential growth, i.e., $g_+ = 0$, $g_- = -2G_0\Omega_0/\omega_0$, and $b_\pm/a_\pm \approx -1$. The condition $\Delta k = 0$ defines the propagation angle for perfect phase matching, i.e.,

$$\cos\theta_0 \approx 1 - \frac{\beta_2 \Omega_0^2}{2k_0} - \frac{(n_K + n_R) I_0}{n_0}\left(\frac{\Omega_0}{\omega_0}\right)^2, \tag{29}$$

where the angle is defined with respect to the z-axis and it has been assumed that $|k_\pm| \ll k_0$ and $\Omega_0/c \ll k_0$. For a laser with wavelength 1 μm and intensity $I_0 \sim 10^7$ W/cm^2 propagating in air, the group velocity dispersion term in Eq. (29) provides the dominant deviation from unity; the magnitude of the phase matching angle is typically $\theta_0 \approx 2\times 10^{-5}$ rad.

Figure 2 plots the growth rate versus propagation angle for various values frequency mismatch $\Delta\bar{\omega} \equiv (\omega - \Omega_0)/\Omega_0$. The growth rate is calculated using Eq. (20) with $\Omega_0 = 1.4\times 10^{13}$ sec^{-1}, $\Gamma_2 = 10^{10}$ sec^{-1}, $n_R = n_K = 3\times 10^{-19}$ cm^2/W, $\beta_2 = 1.6\times 10^{-31}$ sec^2/cm, $I_0 = 10^7$ W/cm^2, and $\lambda = 1\ \mu$m. The angle at which the growth rate goes to zero corresponds to the condition for perfect phase matching ($\Delta k = 0$). At resonance ($\Delta\bar{\omega} = 0$), there is a small, but nonzero growth rate for direct forward scattering. As the propagation angle increases from zero to θ_0, the growth rate decreases. As the angle increases beyond θ_0 the growth rate increases and saturates at the maximum value, $g = G_0$, which corresponds to the regime where the Stokes and anti-Stokes waves are decoupled. For frequencies slightly below resonance, there is a local maximum in the region $\theta > \theta_0$. For frequencies slightly above resonance, a local maximum can occur in the region $\theta < \theta_0$.

B. Modulational instability (MI)

In the absence of the Raman effect, a modulational instability [17,18] can occur in regions of anomalous dispersion, i.e., when $\beta_2<0$. This instability results from a longitudinal compression of energy due to the interplay of self-phase modulation (Kerr nonlinearity) and group velocity dispersion. To derive the growth rate for this instability, we set $n_R=0$ and assume $\omega \ll \omega_0$. With these assumptions, Eq. (20) reduces to

$$g_{\pm}=\pm\left[\kappa_0^2-\kappa_0-\frac{1}{2}\left(\beta_2\omega^2-\frac{k_\perp^2}{k_0}\right)\right]^{1/2}. \tag{30}$$

Setting $k_\perp=0$, Eq. (30) shows that a modulational instability is possible when $\beta_2<0$ and $0<|\omega|<\sqrt{2}\omega_{MI}$, where $\omega_{MI}\equiv\sqrt{2\kappa_0/|\beta_2|}$ is the frequency shift at which the growth rate is maximum. For $\omega=\pm\omega_{MI}$, we have $g_{\pm}=\pm\kappa_0$. For the exponentially growing $(+)$ mode, Eq. (21) yields, $a_+/b_+\approx i$, which indicates that the Stokes and anti-Stokes signals asymptotically have equal amplitudes, but are out of phase by $\pi/2$.

C. Filamentation instability (FI)

The filamentation instability results in the transverse break up of a laser beam into filaments due to the self-focusing effect of the Kerr nonlinearity. The growth rate for the FI can be obtained from Eq. (30). Setting $\beta_2=0$, it is found that an instability exists for wave numbers $0<|k_\perp|<\sqrt{2}k_{FI}$, where $k_{FI}\equiv\sqrt{2\kappa_0 k_0}$ is the transverse wave number at which the growth rate is maximum. For $k_\perp=\pm k_{FI}$, the growth rate is $g_{\pm}=\pm\kappa_0$. Using Eq. (21) it can be shown that, similar to the MI, $a_+/b_+\approx i$ at maximum growth.

V. NUMERICAL SIMULATIONS

A numerical simulation based on solving Eq. (4) together with the stimulated Raman response given by Eqs. (5) has been developed at NRL. The simulation renders the laser pulse envelope on a three-dimensional Cartesian (x,y,τ) grid. The laser pulse is advanced in z according to Eq. (4) using a split-step spectral method [18] in which the linear terms are advanced in Fourier space and the nonlinear terms handled in coordinate space. The equations describing the Raman response are solved at each z step by a fourth-order Runga-Kutta integration. The following simulations (a) benchmark the numerical simulation with the analysis of Sec. IV, (b) address the effects of pulse duration on Raman gain, (c) show the 3D evolution of laser pulses under the influence of Raman scattering, and (d) illustrate the interpulse Raman interaction of a pulse train. The laser pulse parameters used in the following examples are characteristic of a rf linac-driven MW-class FEL.

A. Benchmarking of the numerical code

The first set of simulations establishes the validity of the numerical code by recovering the correct analytic properties of the Raman instability in the strongly and weakly coupled regimes as described in Sec. IV A. To facilitate the comparison between analysis and simulation, the transverse variation of the laser envelope was neglected. The parameters describing the Raman medium are taken to be $\omega_R=1.4\times10^{13}$ sec^{-1}, $\Gamma_2=2\times10^{11}$ sec^{-1}, $n_K=5.6\times10^{-19}$ cm^2/W, $n_R=10^{-18}$ cm^2/W, and $\beta_2=1.6\times10^{-31}$ s^2/cm. These parameters are similar to those of air except that the damping rate Γ_2 is a factor of 20 larger and the Raman index is a factor of 100 larger than the measured values for long ($\sim$nsec) pulses. These parameters were chosen to properly resolve the long pulse limit in which the analysis is valid and, at the same time, keep the simulation run time from becoming prohibitive. The initial laser pulse envelope is given by $A(z=0,\tau)=(A_0+\delta A)f(\tau)$. The function $f(\tau)$, illustrated in Fig. 3, describes a longitudinal pulse profile with rise and decay times of τ_0, and a constant mid-section of duration τ_L. For the benchmarking simulations, the rise time $\tau_0=70T_R$, and the pulse duration $\tau_L=100T_R$, where $T_R=2\pi/\omega_R$. The pump laser has wavelength $\lambda=1$ μm. The initial $(z=0)$ perturbation δA has the form of Eq. (13a) with $k_\perp=0$, $\omega=\omega_R$, $A_+=-A_-$, and $|A_\pm|/A_0=10^{-7}$.

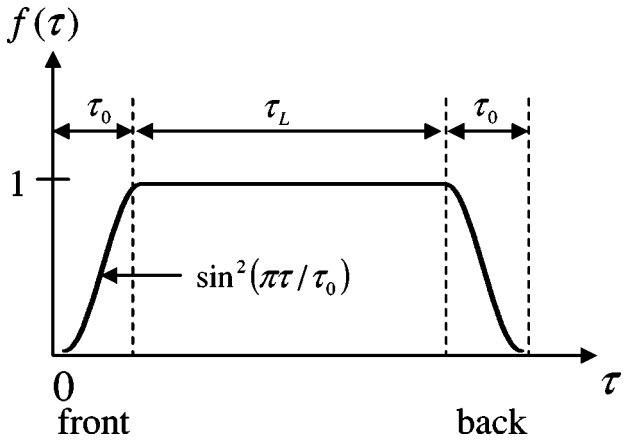

FIG. 3. Schematic diagram of the initial longitudinal laser envelope profile used in the simulation results shown in Fig. 4 and Figs. 6–10.

According to the analysis of Sec. IV A, the coupling between Stokes and anti-Stokes waves is determined by the ratio $|\Delta k|/G_0$. For these simulations, this ratio is varied by changing the laser intensity. The amplitudes of the Stokes and anti-Stokes waves are determined by taking a Fourier transform in τ of the laser envelope within the flat region of the pulse away from the leading and trailing edges where transient effects could affect the comparison between theory and simulation.

Figure 4 shows the results of simulations of the Raman instability in the weakly and strongly coupled regimes. For the simulation in the weakly coupled regime [Fig. 4(a)] $I_0=2\times10^5$ W/cm^2, corresponding to $|\Delta k|/G_0\sim64$. For the strongly coupled regime [Fig. 4(b)], $I_0=2\times10^8$ W/cm^2, corresponding to $|\Delta k|/G_0\sim0.06$. In both cases the growth rates obtained from the simulation are in excellent agreement with the analytic result given by Eq. (25). It is also consistent with the analysis that in the weakly coupled regime, the amplitude of the anti-Stokes wave is much smaller than that of

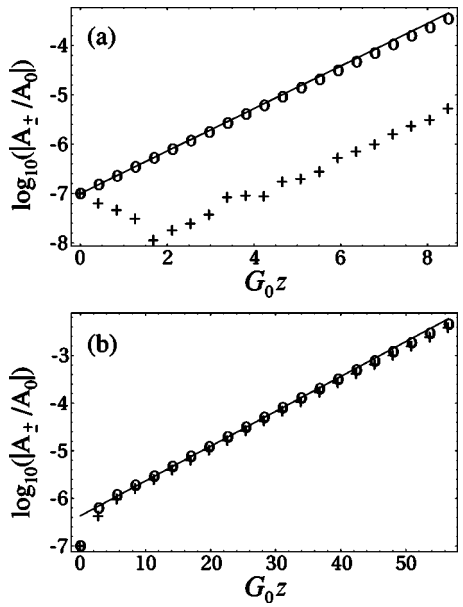

FIG. 4. Normalized Stokes (o) and anti-Stokes (+) amplitude vs normalized propagation distance in (a) the weakly coupled regime ($|\Delta k|/G_0 \sim 64$) and (b) the strongly coupled regime ($|\Delta k|/G_0 \sim 0.06$) obtained from 1D, long-pulse, simulations with $\Omega_0 = 1.4\times10^{13}$ sec^{-1}, $\Gamma_2 = 2\times10^{11}$ sec^{-1}, $n_K = 6\times10^{-19}$ cm^2/W, $n_R = 10^{-18}$ cm^2/W, and $\beta_2 = 1.6\times10^{-31}$ s^2/cm. Laser pulse parameters are $\lambda = 1\ \mu$m, $\tau_0 = 70T_R$, and $\tau_L = 100T_R$, where $T_R = 2\pi/\omega_R$. The peak laser intensity is $I_0 = 2\times10^5$ W/cm^2 for panel (a) and $I_0 = 2\times10^8$ W/cm^2 for panel (b). The solid curve denotes the corresponding analytic Stokes amplitude with the growth rate given by Eq. (25).

the Stokes wave, while in the strongly coupled regime, the Stokes and anti-Stokes waves have comparable amplitudes.

In other simulations, the results of which will be published elsewhere, the transverse dynamics of the numerical code were also successfully benchmarked by comparing the growth rate of the filamentation instability with the analysis of Sec. IV C.

B. Effect of pulse duration on Raman gain

The next set of simulations shows the effects of pulse duration on Raman growth in the linear regime for single pulses. To isolate effects due to the Raman process, linear diffraction and the nonlinearity due to bound electrons (the Kerr nonlinearity) is neglected in these simulations. The paraxial approximation is also made so that the term in Eq. (4) containing the mixed derivative is neglected. Group velocity dispersion, which is important for short pulses, is retained.

The initial pulse envelope is taken to be Gaussian in the temporal coordinate, i.e., $A(z=0,\tau) = A_0 \exp(-\tau/\tau_L)$ with no transverse variation (1D). The laser wavelength $\lambda = 1\ \mu$m. The parameters describing the Raman response are taken to be $\omega_R = 1.4\times10^{13}$ sec^{-1}, $\Gamma_2 = 10^{10}$ sec^{-1}, and gain coefficient $G = 2.5$ cm/TW. The GVD parameter $\beta_2 = 1.6\times10^{-31}$ sec^2/cm.

In what follows, the pulse duration τ_L and peak intensity I_0 are varied, keeping the product $\tau_L I_0 = 10^{-4}$ W s/cm^2, which is proportional to the pulse energy, constant. For example, in these simulations, a 1 psec pulse would span $\omega_R\tau_L/2\pi = 2.7$ rotational periods and have a peak intensity of 10^8 W/cm^2. For pulses that are long compared with the Raman period ($\omega_R\tau_L/2\pi \approx 20$), the initial Fourier width of the laser spectrum is narrow compared with the rotational frequency. Hence, initially there is a much smaller amplitude signal at the Stokes frequency for longer pulses compared with shorter pulses ($\omega_R\tau_L/2\pi \approx 1$) which have a broader spectrum. In the long pulse regime, the Stokes wave can undergo ~ 9 e-foldings before its amplitude is comparable with the amplitude of the main laser, as opposed to the short pulse regime where only ~ 4 e-foldings are required. As the pulses propagate, exponential growth of multiple Stokes lines and lower amplitude anti-Stokes lines shifted from the central laser frequency by harmonics of ω_R are observed. To determine the Raman growth rate, the amplitude of the first Stokes line is measured as a function of propagation distance and fit to an exponential function. Figure 5 summarizes the results of these simulations. The growth rate is seen to increase as the pulse length decreases from $\omega_R\tau_L/2\pi > 20$ to $\omega_R\tau_L/2\pi = 10$. For these longer pulses, transient effects are unimportant and the increase in the growth rate is due to the laser intensity, i.e., the source term for the Raman polarization field, increasing as the pulse length is made shorter. A dramatic reduction in the growth rate is observed when the pulse duration becomes comparable with or less than the rotational period. There are a number of factors which lead to this reduction in the growth rate. First, these shorter pulses are in the transient interaction regime in which the pulse duration is shorter than the temporal growth rate of the Raman instability. Second, group velocity dispersion for these short pulses tends to spread the pulse longitudinally and decrease the intensity, thereby decreasing the source term for the Raman polarization field.

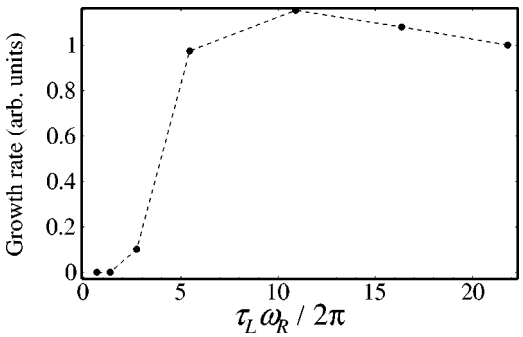

FIG. 5. Results of 1D simulations showing the dependence of the growth rate of the first Stokes line on the pulse length for Gaussian pulses. The peak intensity is varied with the pulse length to keep the fluence constant.

C. 3D simulations

When the transverse variation of the laser envelope is included, the stimulated Raman scattering process can be affected by a number of other 3D effects. For example, phase matching conditions for the Stokes and anti-Stokes waves can cause them to propagate at large angles with respect to

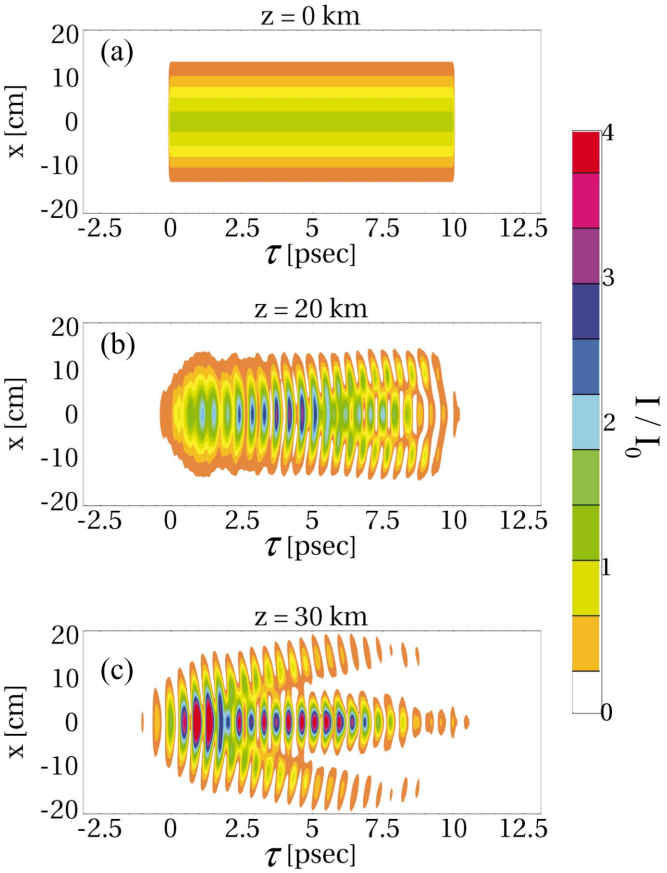

FIG. 6. (Color) Laser intensity contours in air as a function of τ and transverse position (x) at propagation distances (a) $z=0$, (b) $z=20$ km, and (c) $z=30$ km for a laser pulse with an initial Gaussian transverse profile ($r_0=15$ cm) and longitudinal profile indicated by Fig. 4 with $\lambda=1$ μm, $\tau_0=0.1$ psec, $\tau_L=10$ psec, and $I_0=10^7$ W/cm^2.

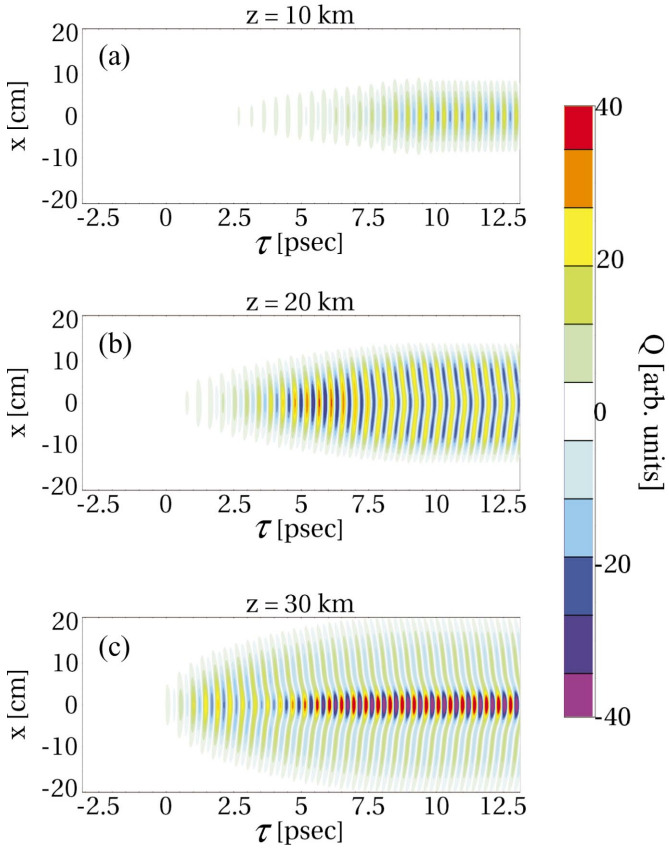

FIG. 7. (Color) Raman polarization function Q, associated with the laser pulse shown in Fig. 5 as a function of τ and transverse position (x) at propagation distances (a) $z=10$ km, (b) $z=20$ km, and (c) $z=30$ km.

the laser propagation axis, thus scattering the laser energy. Also, nonlinear self-focusing can enhance the Raman process by increasing the laser intensity on axis. These effects will be illustrated in the following set of 3D simulations.

For the 3D simulations, the initial laser pulse envelope is given by $A(z=0,r,\tau)=A_0\exp(-r^2/r_0^2)f(\tau)$, where $r=\sqrt{x^2+y^2}$ is the radial coordinate. The function $f(\tau)$ is shown in Fig. 3. The rise time, $\tau_0=\pi/2\omega_R\approx 0.1$ psec, is chosen to be comparable with the rotational Raman period. The transverse profile is a Gaussian with spot size r_0. For these simulations, all of the terms in Eq. (4) are retained. In the two examples presented in this section, we compare the propagation of pulses with durations of 1 psec and 10 psec. For both examples, the initial laser pulse has wavelength $\lambda=1$ μm, spot size $r_0=15$ cm, and an energy of ~ 35 mJ. For the 10 psec example, this corresponds to a peak power of 3.5 GW and a peak intensity of 10^7 W/cm^2. For the 1 psec example, the peak power is 35 GW and the peak intensity is 10^8 W/cm^2.

The nonlinear refractive indicies associated with the bound electron anharmonicty and Raman process are taken to be equal, as indicated by previous short-pulse experiments [12], i.e., $n_K=n_R=3\times 10^{-19}$ cm^2/W. This corresponds to a nonlinear Kerr self-focusing power of $P_{SF}=\lambda^2/(2\pi n_0 n_K)\sim 5.9$ GW due to the bound electron nonlinearity [19]. Hence, the peak power for the 10 psec pulse example is below the threshold for nonlinear self-focusing, while for the 1 psec pulse example, it is above. Experimental determination of P_{SF} for short pulses is discussed in Ref. [20].

1. Long-pulse example

Figures 6 and 7 show, respectively, the contours of the intensity and Raman polarization function Q in the (τ,x) plane ($y=0$) for the 10 psec ($\tau_L\omega_R/2\pi=25$) pulse at various propagation distances. The duration of the initial pulse ($z=0$) is long compared with the rotational Raman period, while the rise time is one-quarter of the rotational period. This initial configuration is favorable for the Raman instability since the sharp rise time optimally excites the Raman polarization field and the long pulse duration contains many rotational periods. Figure 6(a) shows that the polarization function Q is during the early phase of the instability is mainly localized near the axis of the laser pulse and rises in amplitude from the front of the pulse to the back. At $z=20$ km, the laser intensity is strongly modulated at the rotational frequency. From the front to the middle of the pulse, the modulations increase in amplitude. Towards the back of the pulse, the on-axis intensity decreases as laser energy be-

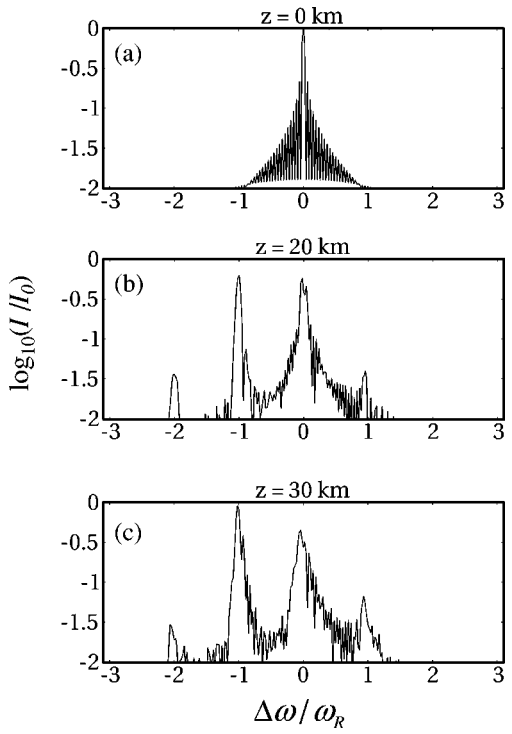

FIG. 8. Frequency spectrum (on axis) of the laser pulse of Fig. 5 at (a) $z=0$ and (b) $z=20$ km, and (c) $z=30$ km showing prominent growth of first and second order Stokes lines.

gins to be scattered off axis. As the pulse propagates, the modulations appear to move forward with respect to the original laser pulse. The Raman polarization field becomes broader in transverse extent [Fig. 7(b)] and continues to increase in amplitude as the instability develops. By $z=30$ km, the intensity modulations, which were initially strongest at the back of the pulse, have grown in amplitude and have moved to the front of the pulse. The modulation, which is characterized by a longitudinal bunching of the laser energy, causes the peak intensity on axis to become larger by a factor of 4 with respect to the initial intensity. Scattering of some of the laser energy off axis is also evident, with the angle of scattering roughly five times larger than the vacuum diffraction angle. At $z=30$ km, the Raman polarization field continues to broaden transversely, but becomes highly peaked on axis.

Figure 8 shows the evolution of the on-axis laser spectrum for the 10 psec pulse. The initial spectrum is narrow compared with the rotational period. The initial signal at the Stokes frequency, $\Delta\omega=-\omega_R$, is two orders of magnitude smaller than the main pump signal at the laser frequency $\Delta\omega=0$. At $z=20$ km, the pump signal has decayed by a factor of 3, and the Stokes wave amplitude has grown to a comparable amplitude. The emergence of a much smaller amplitude second order Stokes line at $\Delta\omega=-2\omega_R$ and first order anti-Stokes line at $\Delta\omega=\omega_R$ is observed. At $z=30$ km, a broadening of the carrier, Stokes, and anti-Stokes lines is observed. The amplitude of the Stokes line is greater than that of the pump. It is evident that the intensity modulations shown in Fig. 6 are associated primarily with the lower frequency Stokes wave, which because of the dispersive properties of air at ~ 1 μm, have a larger group velocity than the main laser pulse. Hence, the prominent growth of the Stokes wave is consistent with the observation that the laser intensity modulations travel forward with respect to the pulse.

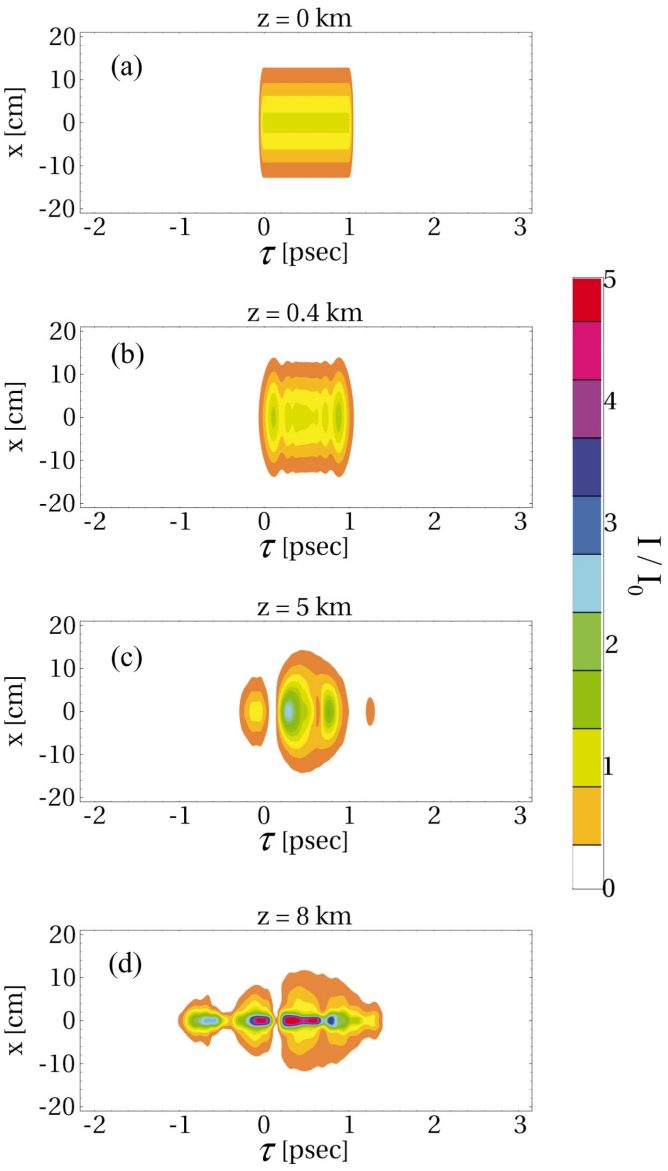

FIG. 9. (Color) Laser intensity contours in air as a function of τ and transverse position (x) at propagation distances (a) $z=0$, (b) $z=0.4$ km, (c) $z=5$ km, and (d) $z=8$ km for a laser pulse with an initial Gaussian transverse profile ($r_0=15$ cm) and a longitudinal profile indicated by Fig. 4 with $\lambda=1$ μm, $\tau_0=0.1$ psec, $\tau_L=1$ psec, and $I_0=10^8$ W/cm^2.

2. Short-pulse examples

The first short-pulse example is for a ~ 1 psec ($\tau_L\omega_R/2\pi=2.5$) laser pulse with the same spot size and energy as in the long-pulse example discussed previously. Figure 9 shows the intensity contours for the short pulse in the (t,x) plane at $y=0$ for propagation distances of $z=0$, 0.4 km, 5 km, and 8 km. At $z=0.4$ km, the pulse becomes

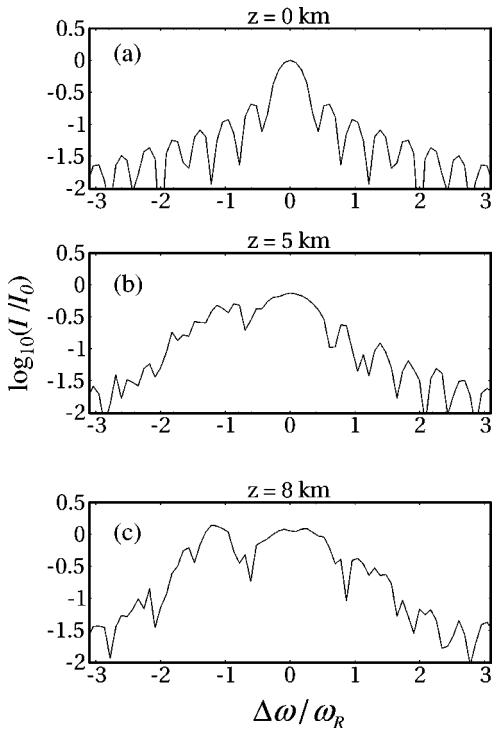

FIG. 10. Frequency spectrum (on axis) of the laser pulse of Fig. 7 at (a) $z=0$ and (b) $z=5$ km, and (c) $z=8$ km.

modulated due to the longitudinal spreading out of the front and trailing portions of the pulse by group velocity dispersion. The modulation frequency in this early stage of propagation is noticeably larger than the rotational frequency. A growing modulation at the rotational frequency becomes apparent at $z\sim 1$ km. At $z=5$ km, the laser intensity is strongly modulated at the rotational frequency and has gained a factor of ~ 2 in intensity on axis. Similar to the long-pulse example, the modulations appear to travel faster than the main laser pulse. At $z=8$ km, the modulations have surpassed the front edge of the main laser pulse causing an apparent longitudinal spreading of the laser. No significant transverse spreading of the laser pulse is observed in this example.

The evolution of the on-axis frequency spectrum is shown in Fig. 10. Because of the shorter pulse duration, there is a much larger amplitude signal at the Stokes frequency initially compared with case of the longer pulse. Hence, fewer e-foldings of the Stokes wave are required to saturate the Raman process and the pulse becomes highly distorted in at a much shorter propagation distance relative to the long-pulse example. Similar to the long-pulse example, it is seen that the intensity modulations are due to primarily to the growth of the Stokes wave, although in the case of the shorter pulse, the spectral width of the Stokes line is very broad.

Another simulation was performed with a shorter 0.5 psec pulse, again, keeping the spot size and pulse energy the same as the previous two simulations. In this case, although the peak intensity was large (2×10^8 W/cm^2) and small amplitude modulations at the rotational frequency developed, these modulations did not grow appreciably as the pulse propagated. Propagation was dominated by group velocity dispersion which resulted in an almost symmetric longitudinal spreading of the entire pulse and a corresponding decrease in peak intensity. The pulse duration was observed to double after propagating ~ 0.5 km.

D. Raman scattering in pulse trains

The following simulations illustrate the interpulse interaction of a pulse train characteristic of a MW-class FEL. In a pulse train, the Raman polarization field excited by the leading pulses can affect the propagation of trailing pulses provided that the pulse separation is not much greater than the characteristic Raman relaxation time, which, in the absence of significant population inversion, is given by $1/\Gamma_2$. For pulse separations less than $1/\Gamma_2$, the Raman polarization fields excited by a train of pulses can interfere constructively, thus amplifying the field and providing a greater seed for instability in trailing pulses. For the pulse train of a MW-class FEL generated by a RF linac, the pulse separation is expected to be about 1 nsec, which is 10 times the relaxation time. Hence, for this pulse configuration, interpulse interactions are expected to be negligible, although more detailed experimental measurements of the Raman relaxation time for $\sim$psec pulses are required to verify this. For the purpose of this study, we consider separation times (~ 0.2 nsec) comparable to the relaxation time to enhance pulse interaction effects.

Because of computational limitations, these simulations are carried out on a two-dimensional (2D), (τ,x) grid. The pulses are slablike, varying transversely in only one coordinate. In this situation the nonlinear focusing properties can differ significantly from fully 3D simulations when the propagation distances become comparable with the nonlinear focal length given by $Z_{NL}=Z_R/\sqrt{P_0/P_{\mathrm{SF}}-1}$ [19], where $Z_R=n_0\pi r_0^2/\lambda$ is the Rayleigh length, and P_0 is the peak power. Hence, we consider examples where the pulse power $P_0<P_{\mathrm{SF}}$ (to avoid Kerr self-focusing) and propagation distances $z<Z_R$. The simulation box is split up longitudinally into individual cells, each containing a single pulse in the train. Provided that no laser energy reaches the front or back cell boundaries, Eqs. (5) for the Raman response can be solved analytically at the cell interfaces to model the decay of the polarization field (both amplitude and phase) over arbitrary durations. The only information required for the analytic calculation is the amplitude and phase of the polarization field at the front of the cell boundary.

In the pulse train example shown here, each pulse is initially identical to the pulse shown in Fig. 6(a). The simulation box is shown schematically in Fig. 11(a). Each pulse is 10 psec in duration. The vertical dashed lines denoting the cell boundaries represent breaks of 0.2 nsec in the t axis. The Raman damping time is taken to be $1/\Gamma_2=0.1$ nsec. The Raman polarization field decays by a factor of ~ 8 across the cell boundaries. At a propagation distance of 13 km, there are noticeable differences in intensity modulations in each pulse. The second and third pulses of the train have developed slightly larger amplitude intensity modulations. At $z=30$ km, obvious differences in the transverse profiles of each pulse become apparent.

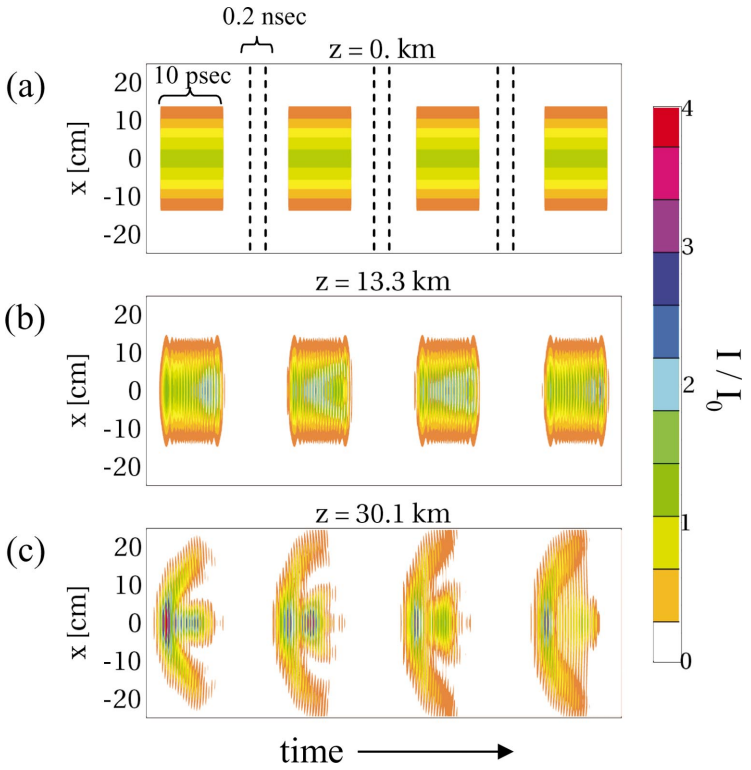

FIG. 11. (Color) 2D simulation of stimulated Raman interaction of a pulse train. Individual pulses at $z=0$ have the same spot size, longitudinal profile, and peak intensity as the initial laser pulse shown in Fig. 5. The pulse separation is 0.2 nsec as shown in panel (a). Note the change in time scale between pulses. Panels (b) and (c) show intensity contours of the pulse train after propagating 13 and 30 km in air, respectively.

VI. CONCLUSIONS

Stimulated rotational Raman scattering of intense picosecond laser pulses in the atmosphere has been investigated using a fully self-consistent, 3D numerical simulation. A key result from this study is that the Raman process can be a sensitive function of pulse format. The high tunability of the FEL makes it suitable for producing the optimal pulse format for propagation. For pulses characteristic of a MW-class FEL, pulses with durations of greater than 10 psec are more prone to scattering than short pulses (<1 psec). For longer pulses, the Raman process can lead to significant off-axis scattering. Subpicosecond pulses are not as prone to scattering but are affected by group velocity dispersion. Group velocity dispersion, however, results in longitudinal redistribution with no transverse scattering of laser energy. Hence, for applications where it is desirable to deliver the maximum amount of laser energy a long distance from the source, it is beneficial to use a short-pulse format to suppress Raman scattering. For pulse trains characteristic of future MW-class FELs, the Raman interaction between pulses may not be important since the pulse separation can be made to be much greater than the assumed Raman relaxation time of 0.1 nsec. More definitive numerical studies, however, require detailed experimental measurements of the Raman parameters of air (rotation frequencies, relaxation times, nonlinear index) for picosecond pulses over a wide range of atmospheric conditions.

ACKNOWLEDGMENTS

This work is sponsored by NAVSEA, the Joint Technology Office in support of the Navy DEW Program Office, and Office of Naval Research.

APPENDIX A: DERIVATION OF THE 3D NONLINEAR PROPAGATION EQUATION

In this appendix we present the derivation of Eq. (4). The starting point is the wave equation for the laser electric field $\mathbf{E}(\mathbf{r},t)$, given by

$$\left(\nabla_\perp^2+\frac{\partial^2}{\partial z^2}-\frac{1}{c^2}\frac{\partial^2}{\partial t^2}\right)\mathbf{E}=\mathbf{S}_L+\mathbf{S}_{NL}\,, \tag{A1}$$

where $\nabla_\perp^2$ is the transverse Laplacian operator and z is the coordinate in the direction of propagation. The quantities $\mathbf{S}_L$ and $\mathbf{S}_{NL}$ denote source terms which are respectively linear and nonlinear in $\mathbf{E}$.

The quantities $\mathbf{E}(\mathbf{r},t)$, $\mathbf{S}_L(\mathbf{r},t)$, and $\mathbf{S}_{NL}(\mathbf{r},t)$ are written in terms of complex amplitudes, $A(\mathbf{r},t)$, $S_L(\mathbf{r},t)$, and $S_{NL}(\mathbf{r},t)$ and a rapidly varying phase, $\psi(z,t)$, i.e.,

$$\mathbf{E}(\mathbf{r},t)=A(\mathbf{r},t)\exp[i\psi(z,t)]\hat{\mathbf{e}}_x/2+\text{c.c.}, \tag{A2a}$$

$$\mathbf{S}_L(\mathbf{r},t)=S_L(\mathbf{r},t)\exp[i\psi(z,t)]\hat{\mathbf{e}}_x/2+\text{c.c.}, \tag{A2b}$$

$$\mathbf{S}_{NL}(\mathbf{r},t)=S_{NL}(\mathbf{r},t)\exp[i\psi(z,t)]\hat{\mathbf{e}}_x/2+\text{c.c.}, \tag{A2c}$$

where $\psi(z,t)=k_0z-\omega_0t$ is the phase, k_0 is the carrier wave number, ω_0 is the carrier frequency, $\hat{\mathbf{e}}_x$ is a transverse unit vector in the direction of polarization, and c.c. denotes the complex conjugate. Substituting Eqs. (A2) into Eq. (A1) yields

$$\left(\nabla_\perp^2-k_0^2+\frac{\omega_0^2}{c^2}+2ik_0\frac{\partial}{\partial z}+2i\frac{\omega_0}{c}\frac{\partial}{\partial t}+\frac{\partial^2}{\partial z^2}-\frac{1}{c^2}\frac{\partial^2}{\partial t^2}\right)A(\mathbf{r},t)$$
$$=S_L(\mathbf{r},t)+S_{NL}(\mathbf{r},t), \tag{A3}$$

where the rapidly varying phase factor has been canceled from both sides of the equation. Although the atmospheric density is spatially varying, the wave number k_0 is taken to be constant since the maximum change in the linear refractive index, i.e., fractional change in wave number, from sea level to vacuum is $\leqslant 10^{-4}$.

Linear source terms

The linear source term which describes effects associated with the linear polarization of bound electrons can be written as

$$\mathbf{S}_L(\mathbf{r},t) = 4\pi c^{-2}\partial^2 \mathbf{P}_L(\mathbf{r},t)/\partial t^2, \tag{A4}$$

where $\mathbf{P}_L$ is the linear polarization field. The relationship between the Fourier transforms of the linear polarization field $\mathbf{P}_L$ and the laser electric field $\mathbf{E}$ is given by $\hat{\mathbf{P}}_L(\mathbf{r},\omega) = \hat{\chi}_L(\mathbf{r},\omega)\hat{\mathbf{E}}(\mathbf{r},\omega)$, where $\hat{\mathbf{P}}_L$ and $\hat{\mathbf{E}}$ are the temporal Fourier transforms of $\mathbf{P}_L$ and $\mathbf{E}$, respectively, and $\hat{\chi}_L(\mathbf{r},\omega)$ is the frequency-dependent linear scalar susceptibility which may also be a function of position.

Following a standard procedure [17,18], the linear source term $S_L(\mathbf{r},t)$ can be rewritten as

$$S_L(\mathbf{r},t) = \left(\frac{\omega_0}{c}\right)^2 \sum_{\ell=0}^{\infty} i^\ell \alpha_\ell(\mathbf{r}) \omega_0^{-\ell} \frac{\partial^\ell A(\mathbf{r},t)}{\partial t^\ell}, \tag{A5}$$

where the unitless coefficient $\alpha_\ell(\mathbf{r})$ is given by

$$\alpha_\ell(\mathbf{r}) = -\frac{\omega_0^{\ell-2}}{\ell!}\frac{\partial^\ell}{\partial \omega_0^\ell}[4\pi \hat{\chi}_L(\omega_0)\omega_0^2]. \tag{A6}$$

In terms of the conventional dispersion parameters β_ℓ [18], defined by $\beta_\ell = \partial^\ell \beta(\omega_0)/\partial\omega_0^\ell$, where $\beta(\omega) = (\omega/c)[1 + 4\pi\hat{\chi}_L(\omega)]^{1/2} = (\omega/c)n(\omega)$, the coefficients are given by

$$\alpha_\ell = -\frac{\omega_0^{\ell-2}}{\ell!}\frac{\partial^\ell}{\partial \omega_0^\ell}[c^2\beta^2(\omega_0) - \omega_0^2]. \tag{A7}$$

For the cases of interest it is sufficient to use the approximation $\beta_1 \approx c^{-1}$.

Nonlinear source terms

The nonlinear source term describes the effects associated with anharmonic motion of the bound electrons and with the transition between rotational states of the N_2 molecules. the nonlinear source term can be written as $\mathbf{S}_{NL}(\mathbf{r},t) = 4\pi c^{-2}\partial^2 \mathbf{P}_{NL}(\mathbf{r},t)/\partial t^2$, where $\mathbf{P}_{NL} = (1/2)P_{NL}(\mathbf{r},t) \times \exp[i\psi(z,t)] + \text{c.c.}$ is the nonlinear polarization field. Factoring out the rapidly varying phase $\exp[i\psi(z,t)]$, the nonlinear source amplitude is due to these effects and can be written as $P_{NL}(\mathbf{r},t) = P_K + P_R$, where the two contributions are described as follows. The nonlinear contribution from bound electrons, i.e., the Kerr effect, is given by [15]

$$P_K(\mathbf{r},t) = \frac{cn_0^2 n_K}{16\pi^2}|A(\mathbf{r},t)|^2 A(\mathbf{r},t), \tag{A8}$$

where n_K is the electronic contribution to the nonlinear refractive index. The nonlinear index defines a self-focusing power due to the Kerr nonlinearity given by [15], $P_{\mathrm{SF}} = \lambda_0^2/(2\pi n_0 n_K)$. The source term due to stimulated molecular Raman scattering is given by (see Appendix B)

$$P_R(\mathbf{r},t) = \chi_L Q(\mathbf{r},t) A(\mathbf{r},t), \tag{A9}$$

where $\chi_L \equiv \hat{\chi}_L(\omega_0)$ is the linear susceptibility evaluated at ω_0 and the unitless Raman polarization function $Q(\mathbf{r},t)$ is determined by solving Eqs. (B11). The Raman source term can also contribute to the third order polarization field.

Nonlinear three-dimensional propagation equation

Substituting Eqs. (A4)–(A9) into Eq. (A3) results in the following nonlinear propagation equation for the laser envelope:

$$\left(\nabla_\perp^2 + \Delta K^2 + 2ik_0\frac{\partial}{\partial z} + \frac{\partial^2}{\partial z^2} + 2i\frac{\omega_0}{c}(1-\alpha_1/2)\frac{\partial}{\partial ct} - (1-\alpha_2)\frac{\partial^2}{\partial c^2 t^2}\right)A(\mathbf{r},t) = -4\pi\frac{\omega_0^2}{c^2}\left(\frac{cn_0^2 n_K}{16\pi^2}|A|^2 + \chi_L Q(\mathbf{r},t)\right)A(\mathbf{r},t), \tag{A10}$$

where the summation in Eq. (A5) has been limited to $\ell \leqslant 3$ and $\Delta K^2 = (1-\alpha_0)\omega_0^2/c^2 - k_0^2$. It proves useful to transform the independent variables from z,t to z,τ, where $\tau = t - z/v_g$ and v_g will be set equal to the linear group velocity of the pulse. In terms of the new variables the derivatives transform as $\partial/\partial t \to \partial/\partial\tau$ and $\partial/\partial z \to \partial/\partial z - v_g^{-1}\partial/\partial\tau$.

The wave number k_0 and group velocity v_g are as yet unspecified. It is convenient to choose them so that the form of the propagation equation is simplified. Choosing $k_0 = (1-\alpha_0)^{-1/2}\omega_0/c = n_0\omega_0/c$ and $v_g = cn_0/(1-\alpha_1) = c/(n_0 + \omega_0\partial n_0/\partial\omega_0)$, the propagation equation simplifies to

$$\left(\nabla_\perp^2 + 2ik_0\frac{\partial}{\partial z} - \frac{2}{v_g}\frac{\partial^2}{\partial z\partial\tau} - k_0\beta_2\frac{\partial^2}{\partial\tau^2}\right)A = -2\frac{\omega_0^2}{c^2}\left(\frac{cn_0^2 n_K}{8\pi}\left|A\right|^2 + 2\pi\chi_L Q\right)A. \tag{A11}$$

Equation (A11) describes the 3D evolution of the complex laser field amplitude, $A(\mathbf{r},\tau)$. The self-consistent model employed here involves the solution of Eq. (A11) along with equations (derived in Appendix B) that describe the Raman response of the medium (air) to the laser field.

APPENDIX B: DERIVATION OF THE RAMAN POLARIZATION FIELD (NONRESONANT SCATTERING)

In this appendix we derive the theoretical model used to incorporate the effects of rotational Raman scattering into the

general nonlinear propagation equation. The model is based on the standard density matrix formalism with an envelope representation for the laser electric field. The envelope representation allows for the generation of a multiwave Raman spectrum, i.e., harmonics of the Stokes and anti-Stokes sidebands, as well as broadening of the individual lines. The model also describes the Raman response in the transient regime and accounts for the natural damping or relaxation of excited states and saturation due to the population depletion of the ground state.

Stimulated Raman scattering can be understood through the energy level diagrams shown in Fig. 1. In our model, the molecular scatterer is assumed to have two rotational eigenstates, 1 (the ground state) and 2, with corresponding energy levels W_1 and W_2, and an excited state, e.g., an electronic or translational state, with energy $W_3 \gg W_2 - W_1$. Defining $\Omega_{nm} = \Omega_n - \Omega_m$, where Ω_n is the frequency associated with state n, it is assumed that the central laser frequency $\omega_0 \neq \Omega_{31}$, Ω_{32}, so that state 3 is not populated, and that Ω_{31}, $\Omega_{32} \gg \omega_0 \gg \Omega_{21}$, where Ω_{21} is the rotational frequency.

The system is also assumed to possess inversion symmetry so that the energy eigenstates possess definite parity. For Raman scattering to occur, the quantities μ_{13} and μ_{32} must be nonzero, where μ_{mn} is the dipole moment matrix element associated with a transition from state m to n. Because of the odd parity of the dipole operator, states 1 and 2 must possess the same parity in order for μ_{13} and μ_{32} to be nonzero. Hence, $\mu_{12} = 0$, indicating that direct transition from 1 to 2 is forbidden so that an intermediate state, e.g., a virtual state, is needed to populate state 2.

Raman Stokes scattering consists of a transition from state (1) to a virtual level associated with state (3) followed by a transition from the virtual level to state (2). In the process, a photon with frequency $\omega_s = \omega_0 - \Omega_{21}$, is emitted. Raman anti-Stokes scattering consists of a transition from state (2) to a virtual state followed by a transition from the virtual state to state (1) thereby emitting a photon of frequency $\omega_a = \omega_0 + \Omega_{21}$. Since the population of state (2) is much smaller than that of state (1) in thermal equilibrium, the anti-Stokes lines are generally much weaker than the Stokes lines [3].

The molecular wave function $\Psi(\mathbf{r},t)$ satisfies the time-dependent Schrödinger equation, $(\hat{H}_0 + \hat{V})\Psi = i\hbar\partial\Psi/\partial t$, where $\hat{H}_0(\mathbf{r})$ is the unperturbed static Hamiltonian operator. The perturbing interaction operator is given by $\hat{V}(\mathbf{r},t) = \hat{\boldsymbol{\mu}} \cdot \mathbf{E}$, where $\hat{\boldsymbol{\mu}} = q\hat{\mathbf{r}}$ is the electric dipole operator. The laser electric field, $\mathbf{E} = E\hat{\mathbf{e}}_\perp$, is given by

$$E(\mathbf{r},t) = (1/2)A(\mathbf{r},t)\exp[i(k_0 z - \omega_0 t)] + \text{c.c.}, \tag{B1}$$

where $A(\mathbf{r},t)$ is the complex amplitude, k_0 is the carrier wave number, ω_0 is the carrier frequency, $\hat{\mathbf{e}}_\perp$ denotes a unit vector in the polarization direction, and c.c. denotes the complex conjugate. The wave function is expanded in terms of the stationary eigenstates of $\hat{H}_0$ according to $\Psi(\mathbf{r},t) = \Sigma_n c_n(\mathbf{r},t)\exp(-i\Omega_n t)u_n(\mathbf{r})$, where $u_n(\mathbf{r})$ are the stationary eigenstates associated with the unperturbed Hamiltonian $\hat{H}_0$, i.e., $\hat{H}_0 u_n = W_n u_n$, and $W_n = \hbar\Omega_n = \int u_n^* \hat{H}_0 u_n d^3r$, is the energy of the nth state. Substituting $\Psi(\mathbf{r},t)$ into the Schrödinger equation, the coefficients c_n are found to satisfy

$$\frac{\partial c_n}{\partial t} = \frac{i}{\hbar}\sum_{m=1}^{3} c_m \mu_{nm} \exp(-i\Omega_{mn}t)E(\mathbf{r},t), \tag{B2}$$

where $\mu_{mn} = \int u_m^*(\mathbf{r})(\hat{\boldsymbol{\mu}} \cdot \hat{\mathbf{e}}_\perp)u_n(\mathbf{r})d^3r$ is the dipole transition moment matrix element and $\Omega_{mn} = \Omega_m - \Omega_n$. The stationary states are normalized such that $\int u_m^*(\mathbf{r})u_n(\mathbf{r})d^3r = \delta_{mn}$, where $m,n = 1,2,3$.

The polarization field is written as $\mathbf{P} \equiv \tilde{P}\hat{\mathbf{e}}_\perp$, where

$$\tilde{P} = N\int \Psi^* \hat{\mu} \Psi d^3r = N\sum_{m,n=1}^{3} \mu_{mn}\rho_{nm}\exp(i\Omega_{mn}t) \tag{B3}$$

contains the fast oscillation at the laser frequency, and where N is the number density of molecules and $\rho_{nm} \equiv c_m^* c_n$ are the density matrix elements. From Eq. (B2) we find that the density matrix elements satisfy

$$\frac{\partial \rho_{nm}}{\partial t} = \frac{i}{\hbar}\sum_{\ell=1}^{3} [\mu_{n\ell}\rho_{\ell m}\exp(i\Omega_{nl}t) - \mu_{\ell m}\rho_{n\ell}\exp(i\Omega_{lm}t)]E(\mathbf{r},t), \tag{B4}$$

where $\rho_{nm} = \rho_{mn}^*$ and $\mu_{nm} = \mu_{mn}^*$. The matrix elements satisfy the conservation law $\rho_{11} + \rho_{22} + \rho_{33} = 1$, where ρ_{nn} represents the fractional population of the nth state (probability that the molecule is in the energy eigenstate n). Since each eigenstate has a definite parity and the dipole operator, $\hat{\boldsymbol{\mu}} = q\hat{\mathbf{r}}$, has odd parity we find that $\mu_{11} = \mu_{22} = \mu_{33} = 0$. In what follows, it is assumed that the laser carrier frequency is such that Ω_{31}, $\Omega_{32} \gg \omega_0 \gg \Omega_{21}$. Since the laser is not resonant with the transition frequencies Ω_{31}, Ω_{32}, state 3 is not populated, i.e., $\rho_{33} = 0$, and we find

$$\rho_{13} \approx \frac{\mu E(\mathbf{r},t)}{\hbar\Omega_{31}}[\rho_{11}\exp(-i\Omega_{31}t) + \rho_{12}\exp(-i\Omega_{32}t)], \tag{B5a}$$

$$\rho_{32} \approx \frac{\mu E(\mathbf{r},t)}{\hbar\Omega_{31}}[\rho_{22}\exp(i\Omega_{32}t) + \rho_{12}\exp(i\Omega_{31}t)]. \tag{B5b}$$

With these approximations the polarization field becomes

$$\tilde{P} = N\mu[\rho_{31}\exp(-i\Omega_{31}t) + \rho_{32}\exp(-i\Omega_{32}t)] + \text{c.c.}, \tag{B6}$$

where $\mu_{13} \approx \mu_{23} = \mu$ is taken to be real. Substituting Eqs. (B5a), and (B5b) into Eq. (B6) the polarization field can be written as $\tilde{P} = \tilde{P}_L + \tilde{P}_R$, where

$$\tilde{P}_L(\mathbf{r},t) = \chi_L E(\mathbf{r},t) \tag{B7a}$$

is the linear polarization field and

$$\tilde{P}_R(\mathbf{r},t) = \chi_L[\rho_{12}\exp(i\omega_R t) + \text{c.c.}]E(\mathbf{r},t), \tag{B7b}$$

is the nonlinear polarization field associated with stimulated Raman scattering. In Eqs. (B7), $\chi_L \equiv 2N\mu^2/(\hbar\Omega)$ is the linear susceptibility, $\Omega = \Omega_{31}$, and $\omega_R = \Omega_{21}$ is the fundamental Raman frequency. In obtaining Eqs. (B7) we used the approximation $\rho_{11} + \rho_{22} \approx 1$, since $\rho_{33} \approx 0$.

From Eq. (B4), we find that

$$\frac{\partial \rho_{12}}{\partial t} = -\Gamma_2 \rho_{12} + i \frac{\mu^2 |A|^2}{2\hbar^2 \Omega} W \exp(-i\omega_R t), \tag{B8a}$$

$$\frac{\partial W}{\partial t} = -(W - W_0)\Gamma_1 + i \frac{\mu^2 |A|^2}{\hbar^2 \Omega} [\rho_{12} \exp(i\omega_R t) - \text{c.c.}], \tag{B8b}$$

where $W = \rho_{22} - \rho_{11}$ is the population difference between levels 2 and 1, $W_0 = W(t \to -\infty)$ (for a medium in which all the molecules are initially in the ground state, $W_0 = -1$), $E^2 = |A(\mathbf{r},t)|^2/2$, i.e., the slowly varying part of E^2 is kept, and Γ_1, Γ_2 are phenomenological damping rates which have been included heuristically. The lifetime of the upper level due to, say, spontaneous radiation, is $1/\Gamma_1$ while the dephasing time for the atomic dipole moment is $1/\Gamma_2$ where Γ_2 is the characteristic transition linewidth.

Equations (B8) can be written in terms of Bloch functions,

$$\frac{\partial U}{\partial t} = \frac{\Omega_R^2}{\Omega} W \frac{|A(\mathbf{r},t)|^2}{A_0^2} \sin(\omega_R t) - \Gamma_2 U, \tag{B9a}$$

$$\frac{\partial V}{\partial t} = \frac{\Omega_R^2}{\Omega} W \frac{|A(\mathbf{r},t)|^2}{A_0^2} \cos(\omega_R t) - \Gamma_2 V, \tag{B9b}$$

$$\frac{\partial W}{\partial t} = -\frac{\Omega_R^2}{\Omega} \frac{|A(\mathbf{r},t)|^2}{A_0^2} [U \sin(\omega_R t) + V \cos(\omega_R t)] - \Gamma_1 (W - W_0), \tag{B9c}$$

where $U = \rho_{12} + \rho_{12}^*$, $V = -i(\rho_{12} - \rho_{12}^*)$, $\Omega_R = \mu A_0/\hbar$ is the Rabi frequency, and A_0 is the peak initial laser electric field amplitude. The Rabi frequency in terms of the initial peak laser intensity, I_0, is $\Omega_R = 2(\mu/\hbar)(2\pi I_0/n_0 c)^{1/2} \approx 5.6 \times 10^8 [I_0(\text{W/cm}^2)]^{1/2}$ (rad/sec). Defining the Raman response function as $Q \equiv 2\,\text{Re}(\rho_{12} e^{i\omega_R t}) = U\cos(\omega_R t) - V \sin(\omega_R t)$, Eqs. (B9) can be written as

$$\frac{\partial^2 Q}{\partial t^2} + (\omega_R^2 + \Gamma_2^2) Q + 2\Gamma_2 \frac{\partial Q}{\partial t} = -\frac{\mu^2}{\hbar^2} \frac{\omega_R}{\Omega} W |A|^2, \tag{B10a}$$

$$\frac{\partial W}{\partial \tau} = \frac{\mu^2/\hbar^2}{\omega_R \Omega} \left(\frac{\partial Q}{\partial \tau} + \Gamma_2 Q \right) |A|^2 - \Gamma_1 (1 + W). \tag{B10b}$$

From Eq. (B9b) and the definition of Q, the Raman polarization field can be written as $\tilde{P}_R(\mathbf{r},t) = P_R(\mathbf{r},t)\exp[i\psi(z,t)]\hat{\mathbf{e}}_x/2 + \text{c.c.}$, in which the slowly varying part is given by $P_R = \chi_L Q(\mathbf{r},t) A(\mathbf{r},t)$.

APPENDIX C: DERIVATION OF COUPLED EQUATIONS FOR STOKES AND ANTI-STOKES FIELDS

Writing the laser envelope and Raman polarization function as $A = A_0 + \delta A$ and $Q = Q_0 + \delta Q$, where the equilibrium quantities are given by Eqs. (12), the linearized equations for the perturbed quantities are given by

$$\left(\nabla_\perp^2 + 2ik_0 \frac{\partial}{\partial z} - \frac{2}{v_g} \frac{\partial^2}{\partial z \partial \tau} - k_0 \beta_2 \frac{\partial^2}{\partial \tau^2} \right) \delta A = -2 \frac{\omega_0^2}{c^2} n_0 \left((2n_K + n_R) I_0 \delta A + \frac{c n_0 n_K}{8\pi} A_0^2 \delta A^* + \frac{2\pi \hat{\chi}_L}{n_0} A_0 \delta Q \right), \tag{C1a}$$

$$\left(\frac{\partial^2}{\partial \tau^2} + 2\Gamma_2 \frac{\partial}{\partial \tau} + \Omega_0^2 \right) \delta Q = \frac{\mu^2}{\hbar^2} \frac{\omega_R}{\Omega} (A_0^* \delta A + A_0 \delta A^*), \tag{C1b}$$

where the dispersion relation for the pump is given by $k_0 = n_0 \omega_0 / c$. Substituting Eqs. (13) into Eqs. (C1) yields

$$\hat{Q}(z) = 2 \frac{\mu^2}{\hbar^2} \frac{\omega_R}{\Omega} \frac{|A_0|}{D(\omega)} [A_-(z) \exp[-i(k_- + \kappa_0) z] + A_+^*(z) \exp[-i(k_+ - \kappa_0) z]], \tag{C2a}$$

$$\left[D_- + k_{NL}^2 + 2ik_0 \left(1 - \frac{\omega}{k_0 v_g} \right) \frac{\partial}{\partial z} \right] A_-(z) = -2 n_0 \frac{\omega_0^2}{c^2} \left(n_K I_0 A_+^*(z) \exp(i\Delta k z) - \frac{\pi \hat{\chi}_L}{n_0} |A_0| \hat{Q}(z) \exp[i(\kappa_0 + k_-) z] \right), \tag{C2b}$$

$$\left[D_+ + k_{NL}^2 + 2ik_0 \left(1 + \frac{\omega}{k_0 v_g} \right) \frac{\partial}{\partial z} \right] A_+(z) = -2 n_0 \frac{\omega_0^2}{c^2} \left(n_K I_0 A_-^*(z) \exp(i\Delta k z) - \frac{\pi \hat{\chi}_L}{n_0} |A_0| \hat{Q}^*(z) \exp[i(\kappa_0 - k_+) z] \right), \tag{C2c}$$

where

$$k_{NL}^2 = 2 \frac{\omega_0^2}{c^2} (2n_K + n_R) I_0,$$

$$D_\pm = \mp 2k_0 k_\pm \left(1 \pm \frac{\omega}{k_0 v_g} \right) - k_\perp^2 + k_0 \beta_2 \omega^2,$$

$$D(\omega) = \Omega_0^2 - \omega^2 + 2i\Gamma_2 \omega,$$

$$\Delta k = k_- - k_+ + 2\kappa_0,$$

$$\kappa_0 = \omega_0 (n_K + n_R) I_0 / c.$$

Substituting Eq. (C2a) into Eqs. (C2b) and (C2c) results in

$$\left[N_+ + 2ik_0\left(1+\frac{\omega}{k_0 v_g}\right)\frac{\partial}{\partial z}\right]A_+(z) = \gamma^*(\omega)[A_+(z)+A_-^*(z)\exp(i\Delta k z)], \quad \text{(C3a)}$$

$$\left[N_- + 2ik_0\left(1-\frac{\omega}{k_0 v_g}\right)\frac{\partial}{\partial z}\right]A_-(z) = \gamma(\omega)[A_-(z)+A_+^*(z)\exp(i\Delta k z)], \quad \text{(C3b)}$$

where $N_\pm \equiv D_\pm + 2k_0\kappa_0$ and $\gamma(\omega) \equiv -2(\omega_0^2/c^2)n_0\{n_K + n_R[\Omega_0^2/D(\omega)]\}I_0$. The condition $N_\pm = 0$ is the dispersion relation which relates ω, $k_\pm$, and $k_\perp$ by

$$k_\pm = \pm\frac{k_0\beta_2\omega^2 - k_\perp^2 + 2k_0\kappa_0}{2k_0(1\pm\omega/k_0 v_g)}, \quad \text{(C4)}$$

from which it follows that

$$\Delta k = 2\kappa_0 - \frac{k_0\beta_2\omega^2 - k_\perp^2 + 2k_0\kappa_0}{k_0(1-\omega^2/k_0^2 v_g^2)}. \quad \text{(C5)}$$

Applying the condition $N_\pm = 0$ allows Eqs. (C3) to be written as

$$\frac{\partial A_+(z)}{\partial z} = G_+[A_+(z)+A_-^*(z)\exp(i\Delta k z)], \quad \text{(C6a)}$$

$$\frac{\partial A_-(z)}{\partial z} = G_-[A_-(z)+A_+^*(z)\exp(i\Delta k z)], \quad \text{(C6b)}$$

where

$$G_\pm \equiv i\frac{\omega_0}{c}\left(1\pm\frac{\omega}{k_0 v_g}\right)^{-1}\left(n_K + n_R\frac{\Omega_0^2}{\Omega_0^2-\omega^2\mp 2i\Gamma_2\omega}\right)I_0. \quad \text{(C6c)}$$

Equations (C6) can be written as

$$\left(\frac{\partial}{\partial z} - G_- + i\frac{\Delta k}{2}\right)F_-(z) = G_- F_+^*(z), \quad \text{(C7a)}$$

$$\left(\frac{\partial}{\partial z} - G_+^* - i\frac{\Delta k}{2}\right)F_+^*(z) = G_+^* F_-(z), \quad \text{(C7b)}$$

where $F_\pm(z) \equiv A_\pm(z)\exp(-i\Delta k z/2)$. Equations (C7) can be combined into a single equation for $F_-(z)$, i.e.,

$$\left(\frac{\partial}{\partial z} - G_+^* - i\frac{\Delta k}{2}\right)\left(\frac{\partial}{\partial z} - G_- + i\frac{\Delta k}{2}\right)F_-(z) = G_- G_+^* F_-(z), \quad \text{(C8)}$$

which can be solved by letting $F_-(z) = F_-(0)\exp(gz)$ and solving for the unknown spatial growth rate g through the equation

$$\left(g - G_+^* - i\frac{\Delta k}{2}\right)\left(g - G_- + i\frac{\Delta k}{2}\right) = G_- G_+^*. \quad \text{(C9)}$$

Equation (C9) has the two solutions

$$g_\pm = \frac{1}{2}\left\{G_- + G_+^* \pm \left[(G_- + G_+^*)^2 - 2i\Delta k\left(G_- - G_+^* - i\frac{\Delta k}{2}\right)\right]^{1/2}\right\}. \quad \text{(C10)}$$

When the two values of g are distinct, the general solution for the Stokes and anti-Stokes wave amplitudes are given by

$$A_-(z) = [a_+\exp(g_+ z) + a_-\exp(g_- z)]\exp(i\Delta k z/2), \quad \text{(C11a)}$$

$$A_+^*(z) = [b_+\exp(g_+ z) + b_-\exp(g_- z)]\exp(-i\Delta k z/2), \quad \text{(C11b)}$$

where the constants $a_\pm$ and $b_\pm$ are determined by imposed boundary conditions and are related by

$$b_\pm = \left(\frac{g_\pm + i(\Delta k/2) - G_-}{G_-}\right)a_\pm. \quad \text{(C12)}$$

The constants $a_\pm$ can be written in terms of the initial ($z=0$) amplitudes $A_-(0)$ and $A_+(0)$, i.e.,

$$a_\pm = \mp\frac{1}{g_+ - g_-}[(g_\mp + i(\Delta k/2) - G_-)A_-(0) - G_- A_+^*(0)]. \quad \text{(C13)}$$

It can be shown using Eq. (C10) that the two solutions for g satisfy the relationship

$$[g_+ - G_- + i(\Delta k/2)][g_- - G_- + i(\Delta k/2)] = -G_- G_+^*. \quad \text{(C14)}$$

Using Eqs. (C12), (C13), and (C14), the coefficients $b_\pm$ can be written as

$$b_\pm = \pm\frac{1}{g_+ - g_-}\{[g_\pm + i(\Delta k/2) - G_-]A_+^*(0) + G_+^* A_-(0)\}. \quad \text{(C15)}$$

Various limiting cases of Eqs. (C10) and (C12) are analyzed in the main body of the paper.

[1] G. R. Neil, C. L. Bohn, S. V. Benson, G. Biallas, D. Douglas, H. F. Dylla, R. Evans, J. Fugitt, A. Grippo, J. Gubeli, R. Hill, K. Jordan, G. A. Krafft, R. Li, L. Merminga, P. Piot, J. Preble, M. Shinn, T. Siggins, R. Walker, and B. Yunn, Phys. Rev. Lett. **84**, 662 (2000).

[2] P. Sprangle, J. Peñano, A. Ting, and B. Hafizi, J. Directed Energy **1**, 73 (2003).

[3] R. W. Boyd, *Nonlinear Optics* (Academic Press, San Diego, 1992).

[4] K. S. Syed, G. S. McDonald, and G. H. C. New, J. Opt. Soc. Am. B **17**, 1366 (2000).

[5] A. P. Hickman, J. A. Paisner, and W. K. Bischel, Phys. Rev. A **33**, 1788 (1986).

[6] V. S. Averbakh, A. I. Makarov, and V. I. Talanov, Sov. J. Quantum Electron. **8**, 472 (1978).

[7] M. Henesian, C. D. Swift, and J. R. Murray, Opt. Lett. **10**, 565

(1985).
[8] M. Rokni and A. Flusberg, IEEE J. Quantum Electron. **22**, 1102 (1986).
[9] N. A. Kurnit and D. E. Watkins, Los Alamos National Laboratory Report No. LAUR 87-0097, 1987.
[10] G. S. McDonald, G. H. C. New, L. L. Losev, A. P. Lutsenko, and M. Shaw, Opt. Lett. **19**, 1400 (1994).
[11] N. Bloembergen *et al.*, Rev. Mod. Phys. **59**, S1 (1987).
[12] E. Nibbering, G. Grillon, M. Franco, B. Prade, and A. Mysyrowicz, J. Opt. Soc. Am. B **14**, 650 (1997); J.-F. Ripoche, G. Grillon, B. Prade, M. Franco, E. Nibbering, R. Lange, and A. Mysyrowicz, Opt. Commun. **135**, 310 (1997).
[13] M. G. Raymer, J. Mostowski, and J. L. Carlsten, Phys. Rev. A **19**, 2304 (1979).
[14] A. P. Hickman and W. K. Bischel, Phys. Rev. A **37**, 2516 (1988).
[15] P. Sprangle, J. Peñano, and B. Hafizi, Phys. Rev. E **66**, 046418 (2002).
[16] M. Mlejnek, M. Kolesik, J. V. Moloney, and E. M. Wright, Phys. Rev. Lett. **83**, 2938 (1999).
[17] P. Sprangle, B. Hafizi, and J. Peñano, Phys. Rev. E **61**, 4381 (2000).
[18] G. P. Agrawal, *Nonlinear Fiber Optics*, 2nd ed. (Academic Press, San Diego, 1995).
[19] P. Sprangle, E. Esarey, and J. Krall, Phys. Rev. E **54**, 4211 (1996).
[20] A. Ting, D. Gordon, D. Kaganovich, E. Briscoe, C. Manka, P. Sprangle, J. Peñano, B. Hafizi, and R. Hubbard, J. Directed Energy (to be published).